metals

MDPI

Article

Melt Processing and Characterization of Al-SiC Nanocomposite, Al, and Mg Foam Materials

Ahmed M. Nabawy [1,*], Khalil Abdelrazek Khalil [2,3], Abdulrahman M. Al-Ahmari [1] and El-Sayed M. Sherif [1,4]

1 Center of Excellence for Research in Engineering Materials (CEREM), advanced Manufacturing Institute (AMI), King Saud University, P. O. Box 800, Riyadh 11421, Saudi Arabia; alahmari@ksu.edu.sa (A.M.A.-A.); esherif@ksu.edu.sa (E.-S.M.S.)
2 Mechanical Engineering Department, King Saud University, P.D. Box 800, Riyadh 11421, Saudi Arabia; kabdelmawgoud@ksu.edu.sa
3 Mechanical Design and Materials Department, Faculty of Energy Engineering, Aswan University, Aswan 81521, Egypt
4 Electrochemistry and Corrosion Laboratory, Department of Physical Chemistry, National Research Centre (NRC), Dokki, 12622 Cairo, Egypt
* Correspondence: ahmed.nabawy@cnl.ca; Tel.: +966-1-1469-9667; Fax: +966-1-1467-0199

Academic Editor: Afsaneh Rabiei
Received: 4 March 2016; Accepted: 5 May 2016; Published: 12 May 2016

Abstract: In the present work, metallic foams of Al, Mg and an Al-SiC nanocomposite (MMNC) have been fabricated using a new manufacturing technique by employing melt infiltration assisted with an electromagnetic force. The aim of this investigation was to study and to develop a reliable manufacturing technique consisting of different types of metallic foams. In this technique, an electromagnetic force was used to assist the infiltration of Al-SiC slurry and of pure liquid metal into a leachable pattern of NaCl, thus providing perfect cellular structures with micro-sized porosities. A high frequency induction coil unit equipped with a vacuum chamber and a hydraulic press was used to manufacture the foam materials. Microstructures of the produced foam materials were explored by using Field Emission Scanning Electron Microscopy (FESEM). The mechanical behavior of the manufactured foams was investigated by applying compression testing. The results indicate a high applicability of the new technique in producing metallic foams of pure metals and of a metal matrix nanocomposite . The produced foam materials displayed isotropic cellular structures with excellent compressive behaviors. Microstructure measurements indicate that the average pore size and strut thickness that can be achieved are in the ranges of 100–500 μm and 50–100 μm, respectively. The produced foam of the Al-SiC nanocomposite material provided the highest strength of 50 MPa prior to the densification stage, which equates to 25 times, and 10 times higher than the strength levels that were obtained by Al, and Mg foams, respectively.

Keywords: manufacturing; metallic foam; nanocomposite; infiltration; electromagnetic stirring

1. Introduction

Metallic foams possess several unique functional properties, such as high energy absorption [1], high strength-to-weight ratio [2], sound absorption [3], electromagnetic shielding [4], and a high specific surface area [5]. The processing routes of metallic foams can be classified into four main technologies: solid state processing [6], liquid state processing [7], electrodeposition and vapor deposition [8]. The liquid state processing route is the most practical method in term of mass production and low production cost. The liquid state processing can be applied by using different methods such as melt gas injection [9], entrapped gas expansion [10], casting using a polymer or wax [11], and metal infiltration through a leachable pattern [12].

Producing metallic foams characterized with high isotropic cellular structures, micro-sized porosities and excellent compressive properties is a challenge due to the randomness of the foaming process. The metal infiltration of the leachable pattern of NaCl is a technique that can grant a certain level of control on the developed foam morphology and structure characteristics. However, the successful metal infiltration requires NaCl with an average particle size larger than 1 mm, as well as a liquid metal having low viscosity. Exploiting NaCl particles with a diameter of less than 1 mm results in an increase of the pressure opposing the infiltration that arises from the capillary pressure, as well as a pressure drop due to the friction between the melt and the NaCl particles [13].

The mechanical behavior of metallic foams is another important aspect to consider when analyzing their performance. The mechanical performance relies on the fabrication quality of the foam material and on certain characteristics of the foam structure such as porosity percentage, strut dimension, and the distribution of pores [14]. The strength of the base metal has a significant effect on the final mechanical properties of metallic foams. Mechanical properties of metallic foams can be evaluated by different testing techniques such as impact [15], tensile [16], three-point bending [17], fatigue [18] and compression [19].

The main purpose of the present study is to introduce a reliable and an advanced manufacturing technique of the metallic foam and to overcome the above mentioned challenges that can be experienced when producing pure metallic and MMNC foam materials. Metallic foams of Al-SiC, pure aluminum, and pure magnesium materials were fabricated by employing a metal infiltration with leachable patterns of NaCl under the stirring effect of electromagnetic forces. The electromagnetic stirring was applied to assist the infiltration process by using finer NaCl particles (<1 mm) and to enable the wetting and incorporation of nano ceramic particles within the melt.

2. Materials and Methods

In the present study, pure aluminum powder (American Elements, 3N grade) with an average particle size of 5 µm, pure magnesium granules (American Elements, 2N grade) with size range of 0.5–1 mm, and SiC nanoparticles with an average particle size of 50 nm (Nanostructured & Amorphous Materials, Inc., Houston, TX, USA) were used. Figure 1 shows micrographs of the aluminum powder, SiC nanoparticles, and NaCl particles. Metallic foams of aluminum, magnesium, and Al-SiC nanocomposite were prepared by employing a developed technique in which the NaCl bed was infiltrated with liquid metal under the effect of electromagnetic stirring. A high frequency induction unit equipped with a vacuum chamber and a press was used to apply induction heating/stirring, thus providing a controlled vacuum atmosphere preventing any oxidation. The Al-SiC nanocomposite was prepared with a ball milling technique in which a mixture of aluminum-10% SiC was mixed with zirconia balls in a weight ratio of 20 balls/1 powder. The ball milling process was carried out at 1000 rpm for 6 h. Sodium chloride particles with a spherical shape and in the size range of 100–500 µm were used in this study as particle space holders to provide the internal cell morphology, as shown in Figure 1c.

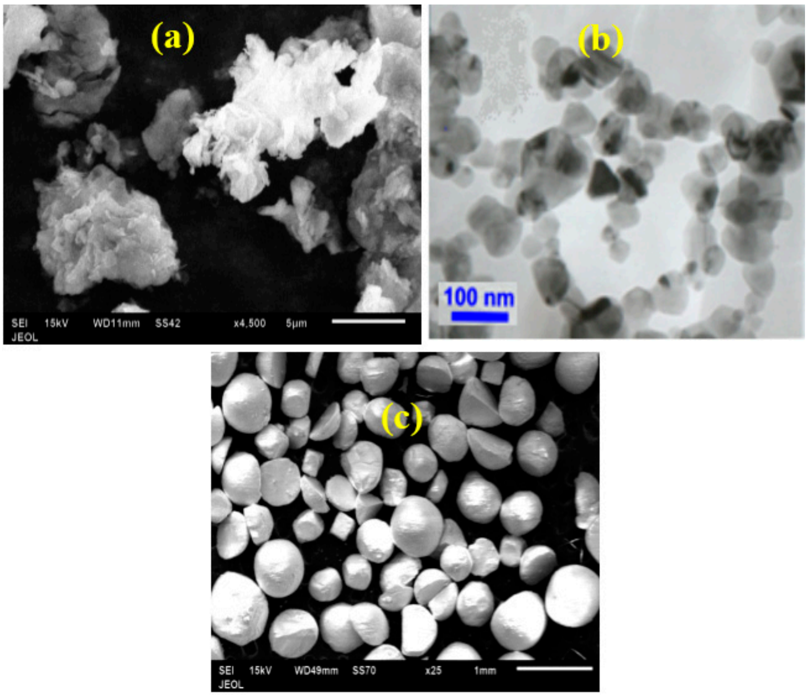

Figure 1. Micrographs of (**a**) pure aluminum powder; (**b**) SiC powder [20] and (**c**) NaCl particles.

Prior to the melting process, the targeted metals of Al, Mg, and Al-SiC were placed in a graphite die (20Ø mm and 40 mm height) above a lower puncher, and then a 3 cm layer of NaCl was added as a second layer above the metal powder. The assembly was then covered from the top with another graphite puncher and placed in the center of the induction coil between a hydraulic press that is contained in a vacuum steel chamber. Figure 2a displays a schematic sketch of the graphite die assembly surrounded by the induction coil. The melting process was started by the passing of an alternating current through the coil, thus providing a strong magnetic field. The magnetic field in turn was in turn applied through the electrically conducting graphite die and through the conducting sample. Figure 2b shows the distribution profiles of the magnetic field and the generated Lorentz force that are roughly calculated throughout the graphite die using Maxwell's equations. Thus, the graphite die also acted as a heating source, and the sample was heated from both the outside and inside. Once the temperature reached the melting points of Al or Mg, the liquid metal (for the pure metal samples) and the viscous slurry of Al-10 wt. % SiC (for nanocomposite samples) were formed. The heating was applied under a vacuum of 1×10^{-3} Torr and at a high heating rate of 700 °C/min. During the melting process, the temperature is continuously measured from the surface of the graphite die using a pyrometer. Under the effect of electromagnetic stirring, the liquid metal and the Al-SiC slurry were enforced to infiltrate the NaCl bed by rising against the gravity direction. The rising of the liquid metal droplets from the tiny gap that is between the upper graphite puncher and the graphite die surfaces was considered as an indication for complete and full infiltration. The induction heating was then turned off and the sample was left to solidify under vacuum. The total time of the induction melting/stirring process of each casting sample is less than 5 min. In the final step of the manufacturing, the compacted NaCl was leached out by soaking the produced sample in warm water for 2 h at 30 °C. Figure 3 shows an example of the final product of the manufactured foam material. Three different castings were prepared per foam material type of Al, Mg, and Al-SiC.

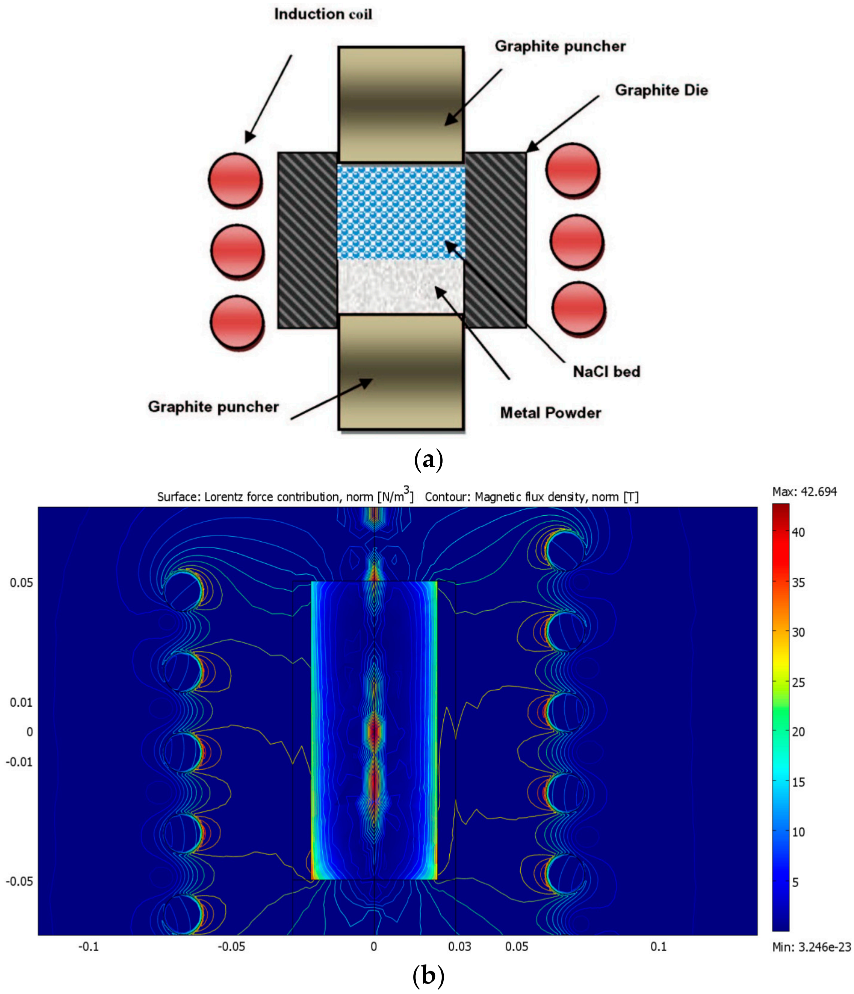

Figure 2. Schematic sketches of (**a**) the graphite die assembly placed in the center of an induction coil, and (**b**) distribution profiles of the magnetic field and Lorentz force throughout the graphite die (using Maxwell's equations).

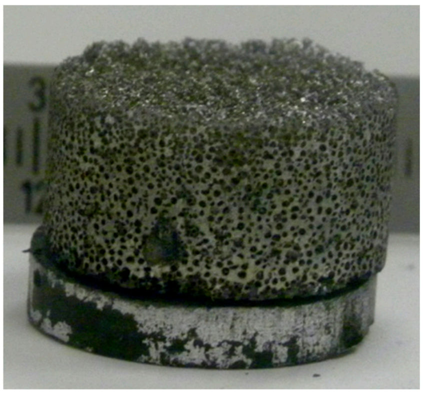

Figure 3. Digital image of a manufactured foam material with 2 cm in height and 2 cm in diameter.

The microstructures of the produced foam were characterized using field emission Scanning electron microscopy (FESEM, KSU, Riyadh, Saudi Arabia) equipped with a secondary electron detector.

The compressive properties of the prepared castings of Al, Mg and Al-SiC were systematically tested using a Lloyd tensile machine (KSU, Riyadh, Saudi Arabia) at a strain rate of 10^{-3} s^{-1}.

The energy absorption of the produced foams was calculated from the area under their stress-strain curves with the following equation:

$$\text{Energy Absorption} = \int_0^s \sigma d\varepsilon$$

where the σ, ε and s are the compressive stress, strain and densification strain, respectively.

3. Results and Discussion

3.1. Microstructure

Figure 4 shows the microstructures of the produced Al, Mg, and Al-SiC foams through the infiltration process under the electromagnetic stirring effect, which were fabricated by using spherical NaCl particles. The foam microstructures display a high isotropy and a uniform distribution of open cells with pores of spherical morphology. The pore morphologies are identical and replicate the typical spherical shape of the space holder particles of NaCl. From FESEM measurements, it is seen that the pore size and cell thickness are in the ranges of 100–500 μm and 50–100 μm, respectively. The number of the pores per inch (PPI) in the produced foam is in the range of 100–125 ± 10. These measurements represent the high efficacy of the present manufacturing technique in producing foam materials characterized with an elevated quality, homogenous cell distribution and micro-sized porosities.

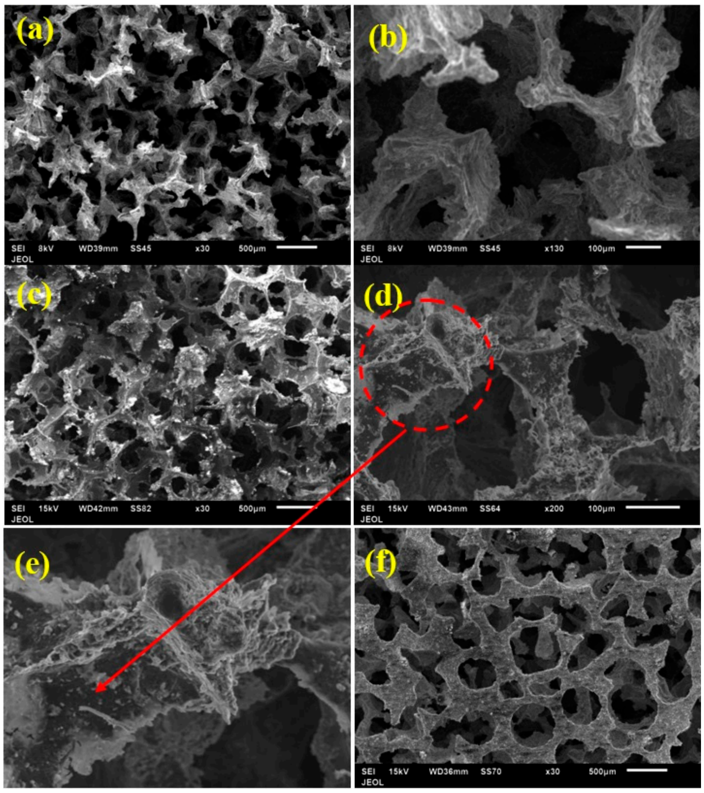

Figure 4. Microstructures of (**a**,**b**) the pure Al foam at different magnifications; (**c**,**d**) the Al-SiC foam at different magnifications; (**e**) a magnified area selected from (**d**); and (**f**) the pure Mg foam.

Reproducing the same cellular morphology of different metals of Al, Mg, and Al-SiC that already display high diversity in melt characteristics (viscosity, fluidity, density, *etc.*) indicates the advantages of utilizing the electromagnetic stirring during the infiltration process. In the magnified FESEM image shown in Figure 4c, it can be observed that the SiC nanoparticles distribute uniformly throughout cell struts indicating perfect wetting and incorporation of SiC nanoparticles within the melt.

The previous studies [13,21] focused on melt processing of metallic foam and reported that the melt infiltration using the NaCl particles with an average particle size smaller than 1 mm is extremely difficult. Decreasing the size of the particle space holder results in an elevated pressure opposing the infiltration due to the capillary pressure and the friction between the melt and NaCl particles. However, in the present manufacturing technique, the electromagnetic stirring improves the infiltration of the liquid metal throughout the micro channels among NaCl particles and the wettability between NaCl and liquid metals. The improved wettability leads to a perfect replication of the spherical morphology of NaCl. As a result of the interaction of the magnetic field formed around the induction coil with the induced current in the sample, the electromagnetic force or Lorentz force is formed. According to Faraday's law, the conductive melt will flow or stir under the effect of the Lorentz force. The stirring effect of the Lorentz force increases the pressure of the liquid metal underneath the NaCl bed that, in turn, reduces the capillary pressure and the NaCl/melt friction. Thus, the liquid metal is enabled to infiltrate the micro-sized channels throughout the NaCl particles in a very short time of less than 1 min.

The electromagnetic stirring not only results in a perfect infiltration but also enables full wetting and incorporation of the nano ceramic particles of SiC with the liquid metal. Incorporation of ceramics into liquid metals is a challenging process during the melt processing of nanocomposites due to poor wettability between ceramic and metal, high clustering tenancy of nano ceramic particles, and high oxidation affinity of liquid metal [22–24]. In the present technique, the electromagnetic stirring results in an elevated shearing force that is able to breakdown clustering and the oxides at melt/ceramic interface, providing an intimate contact between SiC and the melt. Thus, the SiC nanoparticles are perfectly wetted by the melt and then fully incorporated under the continuous stirring effect. This is in full accordance with what was reported in a previous study [25] that consisted of investigating the effect of electromagnetic stirring of the incorporation of the nano TiB_2 particles into an aluminum melt. It was concluded that the electromagnetic force improved the wetting and the incorporation of liquid metal within the melt.

3.2. Compressive Properties

Figure 5 shows the stress-strain curves generated during the compression testing of the produced metallic foams of Al, Mg, and Al-10% SiC. The gradual and uniform deformation shown in the stress-strain curves of the three materials indicate the isotropy and homogenous distribution of the spherical pores of the produced foam structure. The generated stress-strain curves of the processed materials are characterized by three distinguished deformation stages of (i) elastic deformation stage; (ii) plateau deformation stage; and (iii) densification deformation. The elastic deformation and plateau deformation stages of pure aluminum are significantly improved and extended as the SiC nanoparticles are added. It is shown that the densification stage in Al-SiC foam almost starts at a stress level of higher than 50 MPa when compared to ~2 MPa and ~5 MPa for pure aluminum and pure magnesium, respectively. This indicates the superior mechanical behavior of the Al-SiC nanocomposite foam comparing to the pure Al and Mg foam materials.

Uniform deformation of the produced foam can be attributed to the soundness and the isotropic cellular structure of the fabricated foams, which are successfully achieved by applying metal infiltration under the stirring effect of the electromagnetic forces. The electromagnetic stirring not only enables full infiltration of the NaCl bed but also decreases the casting defects in the produced foam. Therefore, the overall compressive behavior of the produced foam is improved. The beneficial effects of the electromagnetic stirring technique in producing a defect-free casting have been reported in different studies [26,27].

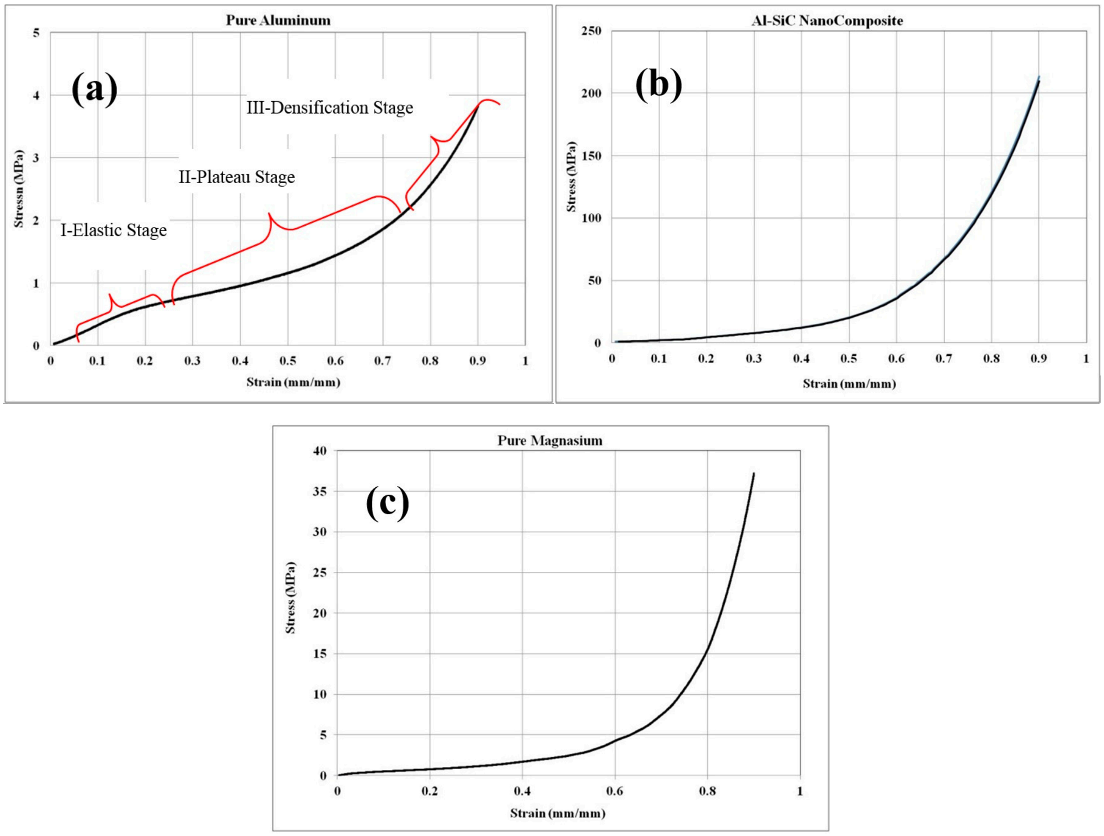

Figure 5. Compressive stress-strain curves of (**a**) pure aluminum foam; (**b**) Al-10% SiC foam (**c**) pure magnesium foam.

The thin strut thickness (50–100 μm) in the produced foam can explain the low strength level that was obtained in the Al- and Mg-foam materials. This is in full harmony with what is stated in other studies [21,28]—that the tiny strut thickness and the high level of the porosity can result in a degraded mechanical behavior. Under applied compressive or tensile stresses, the foam material starts to fail by the cracking of the thin struts that provide the weakest points for crack initiation and propagation. It is obvious that adding 10% of SiC nanoparticles into the aluminum matrix improves the strength and deformation behavior of the struts. According to the Orowan strengthening mechanism, the nano SiC particles act as stiff obstacles, preventing the dislocation movement and the dislocation lines that can only bypass them at higher loading stresses [29,30]. Hence, SiC increases the overall strength of the aluminum matrix of the struts. Figure 6 shows the theoretical strengthening effect of the nano reinforcement particles in respect to the particle size and volume fraction using the following equation:

$$\sigma = M\frac{0.4Gb}{\pi\sqrt{(1-v)}} \cdot \frac{\ln(\frac{\pi R}{2b})}{\lambda}$$

where

M: the Taylor factor for the matrix,
v and G: the poisson ratio of the matrix and shear modulus,
R: the mean radius of the particle,
λ: an effective inter—particle,
b: the Burgers vector.

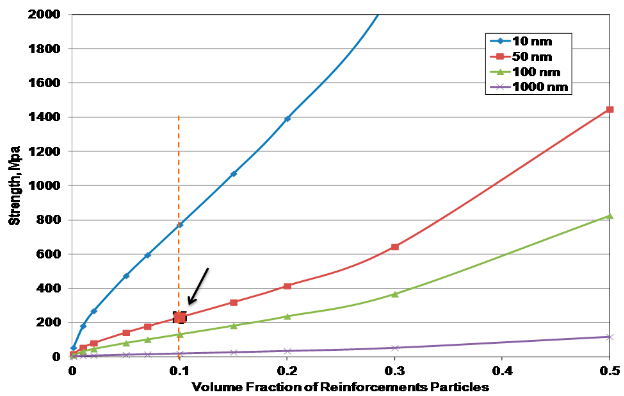

Figure 6. Theoretical strengthening effect of nano reinforcement addition. The arrow points to the theoretical strength level of Al-SiC nanocomposite foam.

From Figure 6, it can be seen that the achieved strength in Al-10% SiC foam (206 MPa at 0.9 stain) is close to the theoretical strengthening effect of SiC nanoparticles (229 MPa) with an average particle size of 50 μm. This can be considered as clear evidence of the full incorporation and the uniform distribution of the SiC particles throughout the aluminum matrix under the stirring effect of electromagnetic forces.

3.3. Energy Absorption

Figure 7 shows the energy absorption of the produced foam materials that were calculated from the area under their stress-strain curves for a strain range of 0.005–0.8. The 0.8 strain level was considered as the onset of the densification stage for all foam materials. It is shown in Figure 7 that the Al-SiC nanocomposite foam material displays a superior level of energy absorption compared to the pure aluminum and pure magnesium foams. The Al-SiC foam material provided an energy absorption of 48 MJ/m^3 compared to 1 MJ/m^3 and 6.4 MJ/m^3 for Al and Mg foam materials, respectively. This indicates the beneficial effect of SiC nano reinforcements in strengthening the foam strut where the foam absorption level of the pure aluminum increased by 48 times. The nano size and uniform distribution of SiC particles results in an improved strength without any degradation in the ductility of the produced foam. The outstanding compressive behavior of the Al-SiC foam can be considered a significant indication for high feasibility of the present manufacturing technique in producing metal matrix nanocomposite foam materials.

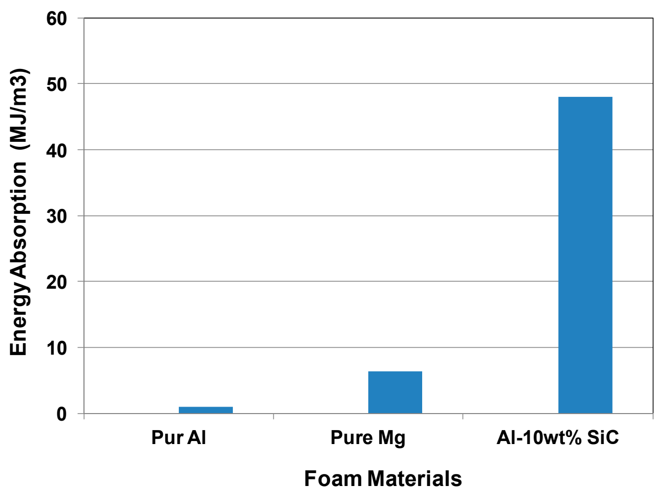

Figure 7. Energy absorption of produced foam materials.

3.4. Fracture Surface

Figure 8 represents a number of morphological features through the fracture surface of the pure Al-foam that indicates the ductile fracture behavior of the struts. In Figure 8a, an overall failure surface is shown. Under compressive stresses, Al-foam deforms in a ductile behavior by creating multiple slip bands at the strut matrix, as displayed in Figure 8. At an extensive level of deformation, cracks start to initiate and propagate throughout the struts, as exhibited in Figure 8b,c. The multiple slip systems result in struts bending and curvy slip lines, as indicated in Figure 8c. It is apparent that struts fail in a ductile manner, which is implemented by extensive localized deformation, and, in some cases, the strut can neck down to a point or bend; this is so clear in Figure 8d.

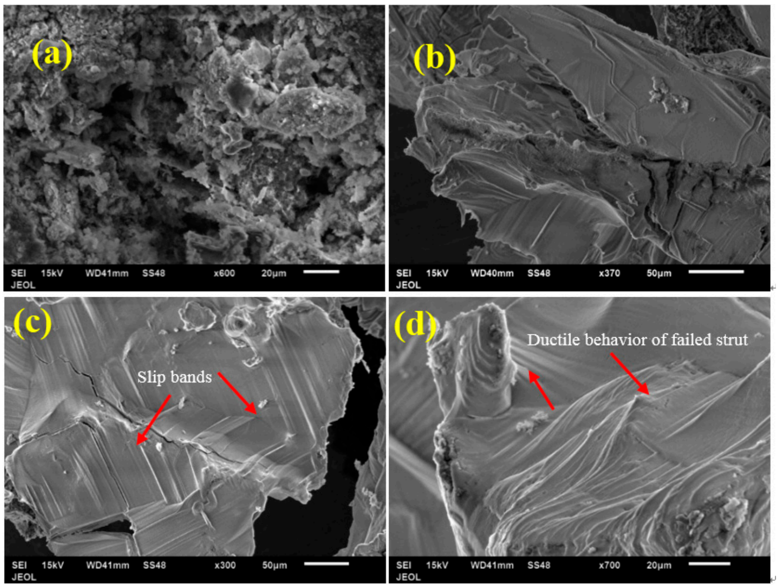

Figure 8. Fracture surface of Al-foam showing different morphologies of: (**a**,**b**) collapsed struts at different magnifications, (**c**) multiple slip systems, and (**d**) necking of the ductile strut.

4. Conclusions

A novel manufacturing technique has been developed to produce metallic foam of the Al-SiC nanocomposite, Al, and Mg characterized with an isotropic structure and an excellent compressive behavior. In this technique, the foam materials were obtained by applying metal infiltration under the stirring effect of electrometric forces. The following conclusions can be drawn:

1. The developed manufacturing technique in the presented study displayed a high applicability in producing different kinds of metallic foams.
2. The metallic foams of Al-SiC, Al, and Mg were successfully manufactured by employing a metal infiltration under the stirring effect of the electromagnetic; thus, forces producing an isotropic foaming structure with micro-sized porosities in the range of 100–500 μm.
3. Addition of 10 wt. % SiC resulted in a significant improvement in the compressive strength of the aluminum foam. The Al-SiC nanocomposite foam provided the highest compressive strength of 50 MPa prior to the densification stage compared to 5 MPa achieved by pure aluminum and 25 MPa achieved by pure magnesium.
4. The produced Al-SiC nanocomposite foam displayed a high level of energy absorption of 48 MJ/m^3 compared to 1 MJ/m^3 and 6.4 MJ/m^3 for Al and Mg foam materials, respectively.
5. The outstanding strengthening effects of SiC nano particles additionally indicate the elevated levels of the wettability and incorporation that can be achieved under the stirring effect of electromagnetic forces.

Acknowledgments: This project was funded by the National Plan for Science, Technology and Innovation (MAARIFAH), the King Abdulaziz City for Science and Technology, and the Kingdom of Saudi Arabia, Award Number (ADV-1853-2).

Author Contributions: Ahmed M. Nabawy and Khalil Abdelrazek Khalil conceived and designed the experiments. Ahmed M. Nabawy and Khalil Abdelrazek Khalil performed the experiments; Ahmed M. Nabawy, Khalil Abdelrazek Khalil and A. M. Al-Ahmari analyzed the data; El-Sayed M. Sherif contributed reagents/materials/analysis tools; Ahmed M. Nabawy and El-Sayed M. Sherif wrote the paper.

Conflicts of Interest: The authors declare no conflict of interest.

References

1. Pinto, P.; Peixinho, N.; Silva, F.; Soares, D. Compressive properties and energy absorption of aluminum foams with modified cellular geometry. *J. Mater. Process. Technol.* **2014**, *214*, 571–577. [CrossRef]
2. Nayyeri, M.J.; Mirbagheri, S.M.H.; Amirkhanlou, S. High strength tailor-made metallic foams (TMFs): Development and characterization. *Mater. Lett.* **2015**, *154*, 152–155. [CrossRef]
3. Li, Y.; Li, Z.; Han, F. Air flow resistance and sound absorption behavior of open-celled aluminum foams with spherical cells. *Procedia Mater. Sci.* **2014**, *4*, 187–190. [CrossRef]
4. Xu, Z.; Hao, H. Electromagnetic interference shielding effectiveness of aluminum foams with different porosity. *J. Alloy. Compd.* **2014**, *617*, 207–213. [CrossRef]
5. Hamadouche, A.; Nebbali, R.; Benahmed, H.; Kouidri, A.; Bousri, A. Experimental investigation of convective heat transfer in an open-cell aluminum foams. *Exp. Therm. Fluid Sci.* **2016**, *71*, 86–94. [CrossRef]
6. He, S.-Y.; Zhang, Y.; Dai, G.; Jiang, J.-Q. Preparation of density-graded aluminum foam. *Mater. Sci. Eng. A* **2014**, *618*, 496–499. [CrossRef]
7. Salvo, L.; Martin, G.; Suard, M.; Marmottant, A.; Dendievel, R.; Blandin, J.-J. Processing and structures of solids foams. *Compt. Rendus Phys.* **2014**, *15*, 662–673. [CrossRef]
8. Wanga, W.; Burgueno, R.; Hong, J.-W.; Lee, I. Nano-deposition on 3-D open-cell aluminum foam materials for improved energy absorption capacity. *Mater. Sci. Eng. A* **2013**, *572*, 75–82. [CrossRef]
9. Zhou, Y.; Li, Y.; Yuan, J. The stability of aluminum foams at accumulation and condensation stages in gas injection foaming process. *Colloids Surf. A Physicochem. Eng. Asp.* **2015**, *482*, 468–476. [CrossRef]
10. Morsi, K.; Daoush, W.M. Al-TiH_2 composite 'particles' as foaming precursors for metallic foams. *Scr. Mater.* **2015**, *105*, 6–9. [CrossRef]
11. Fischer, S.F.; Schüler, P.; Bührig-Polaczek, F. Influence of the casting and mould temperatures on the (micro)structure and compression behaviour of investment-cast open-pore aluminium foams. *Acta Mater.* **2013**, *61*, 5152–5161. [CrossRef]
12. Orbulov, I.N. Metal matrix syntactic foams produced by pressure infiltration—The effect of infiltration parameters. *Mater. Sci. Eng. A* **2013**, *583*, 11–19. [CrossRef]
13. Mizumoto, M.; Murano, T.; Kagawa, A. Microstructure Control of Particle Reinforced Metal Matrix Composites Fabricated by Low-Pressure Infiltration Process. *Mater. Trans.* **2002**, *43*, 2629–2634. [CrossRef]
14. Bekoz, N.; Oktay, E. The role of pore wall microstructure and micropores on the mechanical properties of Cu-Ni-Mo based steel foams. *Mater. Sci. Eng. A* **2014**, *612A*, 387–397. [CrossRef]
15. Peroni, M.; Solomos, G.; Pizzinato, V. Impact behaviour testing of aluminium foam. *Int. J. Impact Eng.* **2013**, *53*, 74–83. [CrossRef]
16. Liu, P.S. Tensile fracture behavior of foamed metallic materials. *Mater. Sci. Eng. A* **2004**, *384*, 352–354.
17. Jiang, B.; Li, Z.; Lu, F. Failure mechanism of sandwich beams subjected to three-point bending. *Compos. Struct.* **2015**, *133*, 739–745.
18. Vendra, L.; Neville, B.; Rabiei, A. Fatigue in aluminum-steel and steel-steel composite foams. *Mater. Sci. Eng. A* **2009**, *517A*, 146–153. [CrossRef]
19. Rajak, D.K.; Kumaraswamidhas, L.A.; Das, S.; Kumaran, S.A. Characterization and analysis of compression load behaviour of aluminium alloy foam under the diverse strain rate. *J. Alloy. Compd.* **2016**, *656*, 218–225. [CrossRef]
20. Nanostructured & Amorphous Materials Inc. Compounds, Silicon Carbide. Available online: http://www.nanoamor.com/inc/pdetail?v=1&pid=621 (accessed on 7 May 2016).

21. Báez-Pimientoa, S.; Hernández-Rojasb, M.E.; Palomar-Pardavé, M.E. Processing and characterization of open-cell aluminum foams obtained through infiltration processes. *Procedia Mater. Sci.* **2015**, *9*, 54–61. [CrossRef]
22. Nogi, K. The role of wettability in metal-ceramic joining. *Scr. Mater.* **2010**, *62*, 945–948. [CrossRef]
23. Zhou, Q.; Zeng, L.; DeCicco, M.; Li, X.; Zhou, S. A comparative study on clustering indices for distribution uniformity of nanoparticles in metal matrix nanocomposites. *CIRP J. Manuf. Sci. Technol.* **2012**, *5*, 348–356. [CrossRef]
24. Nayebi, B.; Bahmani, A.; Asl, M.S.; Rasooli, A.; Kakroudi, M.G.; Shokouhimehr, M. Characteristics of dynamically formed oxide films in aluminum calcium foamable alloys. *J. Alloy. Compd.* **2016**, *655*, 433–441. [CrossRef]
25. Nabawy, A.M.; Zhang, Z.; Chen, X.-G. Synthesis of Al-Tib_2 Nanocomposite Using High Frequency Induction Melting. In Proceedings of Materials Science & Technology 2013, Montreal, QC, Canada, 27–31 October 2013; pp. 1284–1293.
26. Hernández, F.C.R.; Sokolowski, J.H. Comparison among Chemical and Electromagnetic Stirring and Vibration Melt Treatments for Al-Si Hypereutectic Alloys. *J. Alloy. Compd.* **2006**, *426*, 205–212. [CrossRef]
27. Du, Y.; Lu, Y.; Wang, T.; Li, T.; Zhang, G. Effect of Electromagnetic Stirring on Microstructure and Properties of Al0.5CoCrCuFeNi Alloy. *Procedia Eng.* **2012**, *27*, 1129–1134. [CrossRef]
28. Hussain, Z.; Suffin, N.S.A. Microstructure and Mechanical Behaviour of Aluminium Foam Produced by Sintering Dissolution Process Using NaCl Space Holder. *J. Eng. Sci.* **2011**, *7*, 37–49.
29. Zhang, Z.; Chen, D.L. Contribution of Orowan Strengthening Effect in Particulate-Reinforced Metal Matrix Nanocomposites. *Mater. Sci. Eng. A* **2008**, *483–484*, 148–152. [CrossRef]
30. Li, Y.; Zhao, Y.H.; Ortalan, V.; Liu, W.; Zhang, Z.H.; Vogt, R.G.; Browning, N.D.; Lavernia, E.J.; Schoenung, J.M. Investigation of Aluminum-Based Nanocomposites with Ultra-High Strength. *Mater. Sci. Eng. A* **2009**, *527*, 305–316. [CrossRef]